Article:

Luo, P., Yao, W., Susmel, L. orcid.org/0000-0001-7753-9176 et al. (1 more author) (2019) Prediction methods of fatigue critical point for notched components under multiaxial fatigue loading. Fatigue and Fracture of Engineering Materials and Structures, 42 (12). pp. 2782-2793. ISSN 8756-758X

https://doi.org/10.1111/ffe.13116

Prediction methods of fatigue critical point for notched components under multi-axial fatigue loading

Peng Luo[1], Weixing Yao[1,2*], Luca Susmel[3], Piao Li[1]

[1]*State Key Laboratory of Mechanics and Control of Mechanical Structures, Nanjing University of Aeronautics and Astronautics, Nanjing 210016, China*

[2]*Key Laboratory of Fundamental Science for National Defense-Advanced Design Technology of Flight Vehicle, Nanjing University of Aeronautics and Astronautics, Nanjing 210016, China*

[3]*Department of Civil and Structural Engineering, the University of Sheffield, Sheffield S1 3JD, UK*

Abstract: Two methods based on local stress responses are proposed to locate fatigue critical point of metallic notched components under non-proportional loading. The points on the notch edge maintain a state of uniaxial stress even when the far-field fatigue loading is multi-axial. The point bearing the maximum stress amplitude is recognized as fatigue critical point under the condition of non-mean stress, otherwise the Goodman's empirical formula is adopted to amend mean stress effect prior to the determination of fatigue critical point. Furthermore, the uniaxial stress state can be treated as a special multi-axial stress state. The Susmel's fatigue damage parameter is employed to evaluate the fatigue damage of these points on the notch edge. Multi-axial fatigue tests on thin-walled round tube notched specimens made of GH4169 nickel-base alloy and 2297 aluminum-lithium alloy are carried out to verify the two methods. The prediction results show that both the stress amplitude method and the Susmel's parameter method can accurately locate the fatigue critical point of metallic notched components under multi-axial fatigue loading.

Keywords: notched specimen, fatigue critical point, stress gradient, multi-axial fatigue, angle of crack initiation

NOMENCLATURE

a	Notch radius
A	Stress amplitude of local stress response spectrum
B	Mean stress of local stress response spectrum
C_i	i-th loading case
D	Diameter of circular notch
D1	Notched specimens with 1mm diameter circular hole
D2	Notched specimens with 2mm diameter circular hole
E	Young's Modulus
f_{-1}	The fully reverse axial fatigue limit
$f(\sigma_{ij})$	Equivalent stress function.
Δf_{-1}	Range of the fully reverse axial fatigue limit
ΔK_{th}	Range of threshold value for fatigue crack propagation
l_0	Critical distance
R_1	Strain ratio
R_2	Stress ratio
t_{-1}	The fully reverse torsional fatigue limit
V	Volume of fatigue damage area
Y	Notched specimens with waist round hole
ε_a	Normal strain amplitude
θ_1, θ_2	Angle of fatigue critical points
μ	Poisson's ratio
ρ	Loading non-proportional factor of Susmel's fatigue damage parameter
σ_1, σ_2, σ_3	The first principal stress, the second principal stress and the third principal stress respectively
σ_a	Normal stress amplitude of fatigue loading
σ_{FI}	Stress field intensity
σ_n^{max}	Maximum normal stress
σ_r, σ_θ, $\sigma_{r\theta}$,	Three stress components in the polar coordinate
σ_{y1}	Yield strength
τ_a	Shear stress amplitude
φ	Phase angle
$\varphi(\bar{r})$	The weight function
Ω	Region of fatigue damage

1 Introduction

Mechanical metallic components often contain geometrical discontinuities such as keyways, relief grooves, shaft shoulders, bolt holes, etc.. These geometrical features are called notches which can cause not only stress concentration but also stress multi-axiality at notch root even under uniaxial loading.[1-2] Moreover, fatigue cracks generally initiate in the stress concentration regions. It is necessary to study the fatigue behavior of metallic notched components in complex stress field.

For the notched components under uniaxial fatigue loading, the predicted fatigue life tends to be conservative by taking the maximum stress or the maximum strain at the notch root as fatigue damage parameter. Considering the influence of stress gradient, Yao[3] proposed a stress field intensity (SFI) approach to modify the maximum stress at notch root:

$$\sigma_{\mathrm{FI}} = \frac{1}{V}\int_{\Omega} f(\sigma_{\mathrm{ij}})\varphi(\vec{r})\mathrm{dv} \tag{1}$$

where σ_{FI} is the stress field intensity, Ω is the fatigue damage region, V is the volume of Ω, $f(\sigma_{ij})$ is the equivalent stress function which depends on materials, $\vec{r}$ is a vector from the fatigue critical point to any point at notch root, $\varphi(\vec{r})$ is the weight function which represents the contribution of different points in the fatigue damage region to fatigue crack initiation. SFI method is illustrated in Figure 1. This method assumes that fatigue crack initiation is only determined by the stress of some grains at notch root, and the predictions agree well with a large number of test results.[3-5]

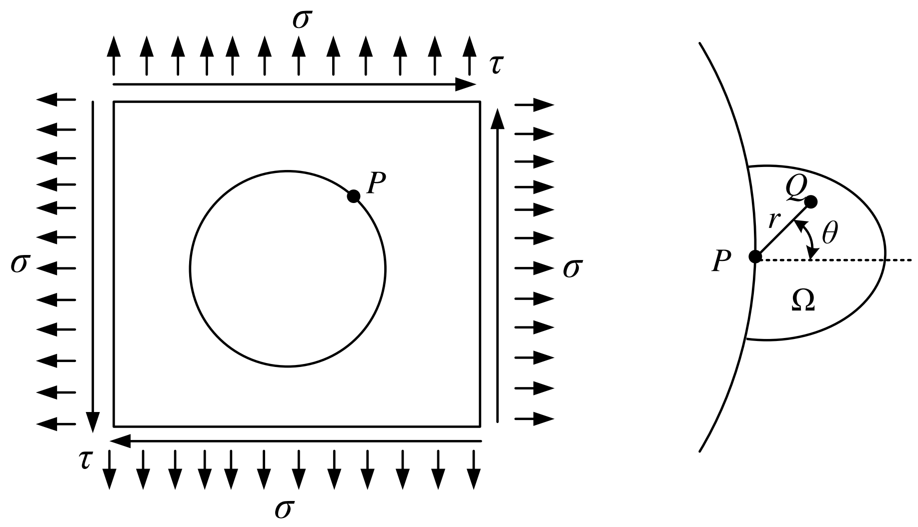

Fig.1 Schematic diagram of stress field intensity method

The Theory of Critical Distance (TCD) was proposed by Tanaka[6] and Taylor[7] on the basis of linear elastic fracture mechanics (LEFM). The critical stress within a characteristic point distance, a line distance, a plane or volume area, in the vicinity of notch, is taken as the fatigue damage parameter to assess fatigue life. This theory is illustrated in Figure 2. According to the topology type, TCD can be divided into four categories. The equations of TCD are[7]:

$$\begin{aligned}
&\text{Point Method: } \sigma_{\mathrm{av}} = \Delta\sigma_1\left(r=\frac{l_0}{2}, \theta=0\right) \\
&\text{Line Method: } \sigma_{\mathrm{av}} = \frac{1}{2l_0}\int_0^{2l_0} \Delta\sigma_1(r,\theta=0)dr \\
&\text{Area Method: } \sigma_{\mathrm{av}} = \frac{2}{1.1\pi l_0^2}\int_{-\pi/2}^{\pi/2}\int_0^{l_0} \Delta\sigma_1(r,\theta)rdrd\theta \\
&\text{Volume Method: } \sigma_{\mathrm{av}} = \frac{3}{2\pi(1.54l_0)^3}\int_0^{2\pi}\int_0^{\pi/2}\int_0^{1.54l_0} \Delta\sigma_1(r,\theta,\varphi)r^2\sin\theta drd\theta d\varphi
\end{aligned} \tag{2}$$

$$\text{EL Haddad equation: } l_0 = \frac{1}{\pi}\left(\frac{\Delta K_{\mathrm{th}}}{\Delta f_{-1}}\right)^2 \tag{3}$$

where l_0 is the critical distance and can be calculated by the EL Haddad[8] empirical equation which is expressed via Eq.(3). Δf_{-1} is the range of fully reversed axial fatigue limit, and ΔK_{th} is the range of threshold value for fatigue crack propagation.

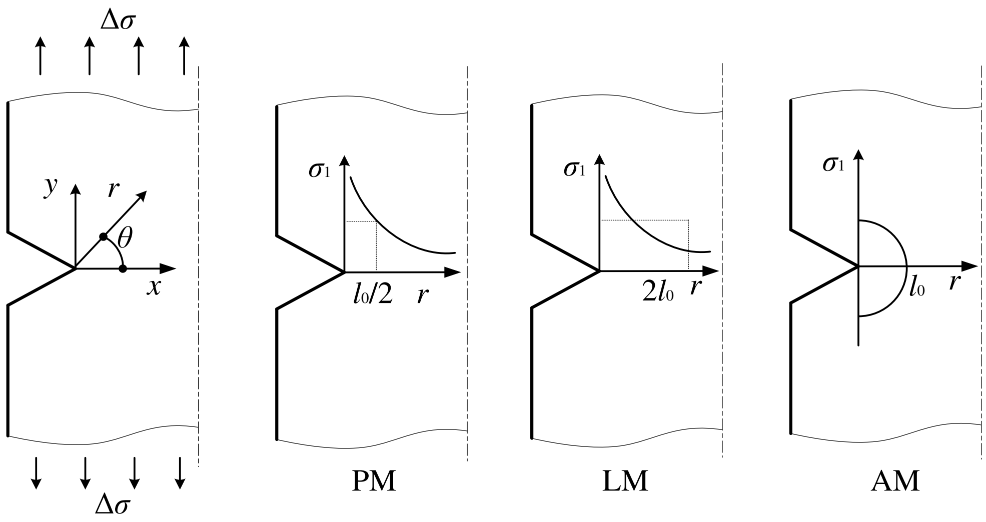

Fig.2 Schematic diagram of PM、LM and AM in TCD

In terms of the crack geometry, both the radius of fatigue damage field $\vec{r}$ in SFI and the critical distance l_0 in TCD are vectors. The fatigue critical point is the starting point of the vectors. In terms of the fatigue damage mechanism, the fatigue critical point is the origin of fatigue crack initiation. Therefore, it is the basis of predicting the fatigue life of notched components under multi-axial fatigue loading to quickly and accurately locate the fatigue critical point.

Chaves *et al.*[9] conducted fatigue tests on thin-walled round tube circular hole notched specimens made of 7075-T6 aluminum alloy under uniaxial tension loading, uniaxial torsion loading and proportional loading. The angle of fatigue crack initiation point was measured after each test. It was found that the fatigue critical point was basically consistent with the position of the maximum principal stress point on the notch edge. Since the axes of principal stress do not change during cyclic loading, the fatigue critical point of notched specimens is consistent with the failure point under static loading, which is the point with the maximum principal stress corresponding to the stress amplitude of fatigue loading, as is shown in Figure 3.

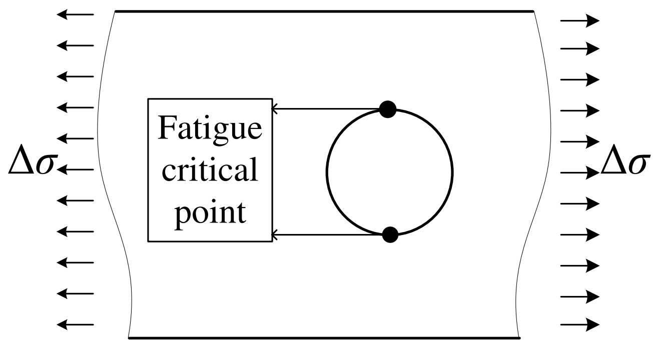

Fig.3 Schematic diagram of fatigue critical point for notches under uniaxial fatigue loading

For notched specimens under non-proportional loading, the axis of principal stress rotates during cyclic loading, which results in the change of the point with the maximum stress on the edge of notch. The notch region of sharp notches, such as V-notch, goes through severe plastic state due to severe stress concentration. The stress amplitude doesn't change much at the notch region, thus the sharp notch root tip can be taken as the fatigue critical point.[10] For blunt notches, such as a circular notch, there is currently no recognized method to locate the fatigue critical point on the edge of notch. Gates *et al.*[11] and Li *et al.*[5] took the fatigue critical point under uniaxial fatigue loading as the fatigue critical point under multi-axial fatigue loading to predict fatigue life. Although the calculation process is simple, the characteristics of non-proportional fatigue loading are not considered in this way. Many fatigue tests have shown that[12-14] the fatigue critical point of notched components under multi-axial fatigue loading is obviously different from that under uniaxial fatigue loading.

The stress amplitude method and the Susmel's parameter method are proposed to locate the fatigue critical point for notched specimens under multi-axial fatigue loading. In addition, constant amplitude multi-axial fatigue tests have been carried out on the thin-walled round tube notched specimens made of GH4169 nickel-base alloy and 2297 aluminum-lithium alloy to verify the two methods. After the fatigue tests, the angles of crack initiation point were measured through an optical microscope. The prediction results show that both the two methods can accurately locate the fatigue critical point of metallic notched components under multi-axial fatigue loading.

2 Experiments

2.1 Material and specimens

GH4169 nickel-base superalloy is a common material used in commercial aero engine. This material shows excellent mechanical and fatigue properties under high temperature and pressure. As a new-generation aluminum alloy independently developed in China, 2297 aluminum-lithium alloy has high specific strength and stiffness and is widely used in aircraft structural design. The chemical composition and mechanical properties of the two materials are shown in Table 1 and Table 2, respectively. The geometric sizes of the three kinds of notched specimens made of GH4169 nickel-base superalloy are shown in Figure 4. The geometric sizes of the two kinds of notched specimens made of 2297 aluminum-lithium alloy are shown in Figure 5. The test specimens are processed by numerically controlled machine tool in order to obtain a qualified surface. The notched specimens with 1-mm-diameter circular hole, 2-mm-diameter circular hole, and waist-round hole are represented by “D1,” “D2,” and “Y,” respectively.

Table1 Chemical composition of GH4169 nickel-base alloy and 2297 aluminum-lithium alloy (wt.%)

Material	Composition									
GH4169 nickel-base alloy	Element	Cr	Nb	Mo	Ti	Co	Al	C	---	---
	percentage	20.0	5.1	3.0	1.0	0.7	0.5	0.07	---	---
2297 aluminum-lithium alloy	Element	Cu	Li	Mn	H	Zr	Fe	Mg	Ti	Si
	percentage	2.82	1.39	0.30	0.20	0.10	0.05	0.03	0.02	0.018

Table2 Mechanical properties of GH4169 nickel-base alloy and 2297 aluminum-lithium alloy

Material	Young’s modulus E/GPa	Poisson ratio μ	Yield strength σ_{y1}/MPa	Fracture strength σ_b/MPa	The fully reverse torsional fatigue limit t_{-1}/MPa	The fully reverse axial fatigue limit f_{-1}/MPa
GH4169 nickel-base alloy	240	0.30	1083	1502	318	574
2297 aluminum-lithium alloy	84.2	0.28	440	480	74.6	126

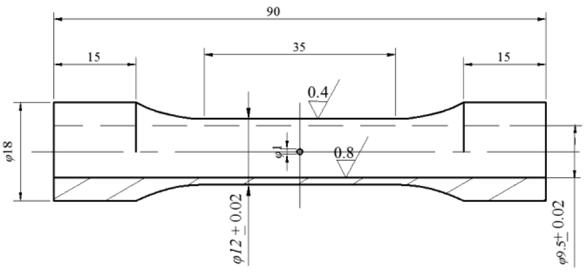

a) D=1mm,circular hole

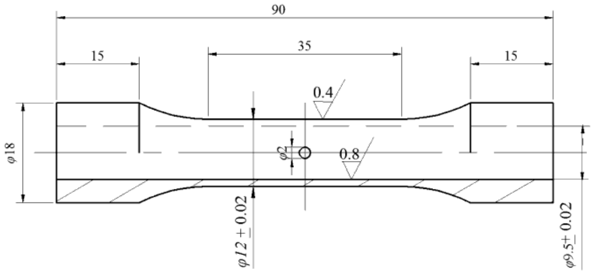

b) D=2mm, circular hole

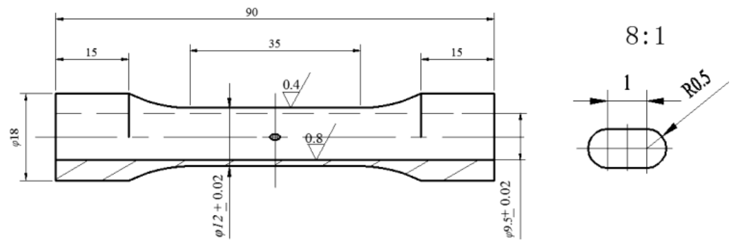

c) waist-round hole

Fig.4 Geometric sizes of notched specimens made of GH4169 nickel-base superalloy

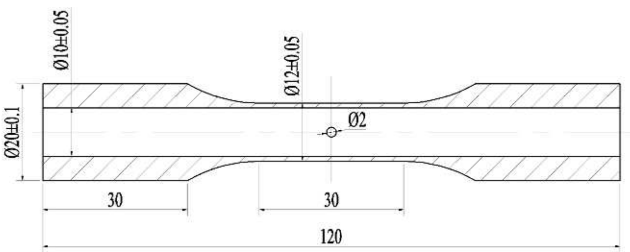

a) D=2mm, circular hole

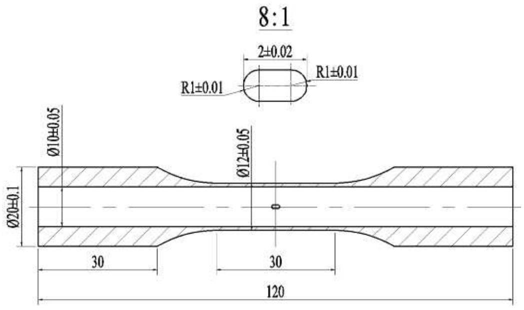

b) waist-round hole

Fig.5 Geometric sizes of notched specimens made of 2297 aluminum-lithium alloy

2.2 Experiments and results

All the tests were performed on MTS809 biaxial fatigue testing machine at room temperature. The testing system was equipped with electro-hydraulic servo control, computer control and data acquisition. It has a capacity of ±100kN in axial load and ±1100 N·m in torque. For the notched specimens made of GH4169 nickel-base superalloy, the MTS632.80F-04 biaxial extensimeter was used for the strain-controlled multi-axial fatigue test with a sine wave. The frequency of fatigue loading is 1Hz and the strain ratio R_1 of fatigue loading is -1. For the notched specimens made of 2297 aluminum-lithium alloy, the stress-controlled multi-axial fatigue test was carried out with a sine wave. The frequency of fatigue loading is 3Hz and the stress ratio R_2 of fatigue loading is 0.1.

After the multi-axial fatigue tests, the angle of the crack initiation point on the notch edge was measured with VHX-1000 3-DVM. Notches are clearly displayed on the computer screen as is shown in Figure 6(*a*). The definition of the angle is shown in Figure 6(*b*). The measured angles of notched specimens made of GH4169 nickel-base superalloy and 2297 aluminum-lithium alloy are summarized in Table 3 and Table 4, respectively.

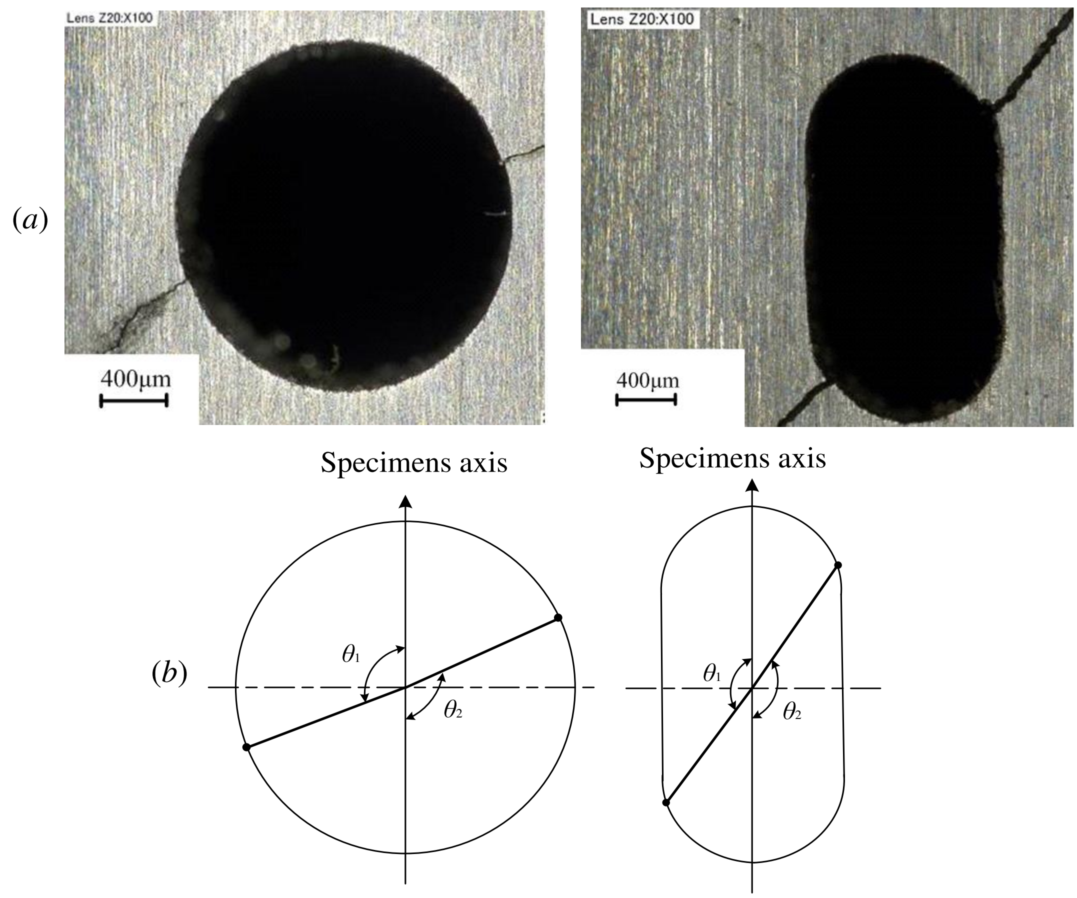

Fig.6 (*a*) The photographs of the notches under VHX-1000 3-DVM; (*b*) Definition of the angle of fatigue critical point for the notches

Table3 Angles of fatigue critical point of notched specimens made of GH4169 nickel-base superalloy (R_1=-1)

Type of notches	Normal strain amplitude ε_a	Shear strain amplitude γ_a	Phase angle φ/°	Specimen No.	Angles of fatigue critical point θ_1/°	Angles of fatigue critical point θ_2/°	Mean value of angle θ_m/°

Type of notches	Normal strain amplitude ε_a	Shear strain amplitude γ_a	Phase angle φ/°	Specimen No.	Angles of fatigue critical point θ_1/°	Angles of fatigue critical point θ_2/°	Mean value of angle θ_m/°
D1	0.123%	0	0	GD1_1	94.0	98.0	93.6
				GD1_2	88.9	---	
	0	0.286%	0	GD1_3	123.0	148.0	128.0
		0.303%		GD1_4	120.0	121.0	
	0.107%	0.107%	45	GD1_5	94.0	101.0	98.0
				GD1_6	---	99.0	
	0.100%	0.200%	45	GD1_7	113.0	112.0	111.4
				GD1_8	116.6	104.0	
	0.130%	0.130%	90	GD1_9	98.0	93.0	95.0
				GD1_10	94.0	---	
D2	0.115%	0	0	GD2_1	101.0	93.7	97.5
				GD2_2	95.2	100.0	
	0	0.303%	0	GD2_3	51.0	36.0	44.0
				GD2_4	46.0	43.0	
	0.122%	0.122%	45	GD2_5	100.1	104.6	104.2
				GD2_6	101.0	111.0	
	0.092%	0.183%	45	GD2_7	108.0	111.0	110.3
				GD2_9	107.0	115.0	
	0.122%	0.122%	90	GD2_9	99.6	---	99.6
				GD2_10	---	---	
Y	0.160%	0	0	GY_1	42.5		40.2
				GY_2	38.0	40.0	
	0	0.277%	0	GY_3	149.0	148.0	148.5
				GY_4	---	---	
	0.139%	0.139%	45	GY_5	142.0	139.5	144.7
				GY_6	139.5	157.7	
	0.104%	0.208%	45	GY_7	143.4	154.0	145.5
				GY_8	142.0	142.5	
	0.139%	0.139%	90	GY_9	140.8	---	143.3
				GY_10	146.7	142.5	

Note: “---” means that no cracks were observed.

Table4 Angles of fatigue critical point of notched specimens made of 2297 aluminum-lithium alloy (R_2=0.1)

Type of notch	Maximum normal stress σ_{max}/MPa	Maximum shear stress τ_{max}/MPa	Phase angle φ/°	Specimen No.	Angle of fatigue critical point θ_1/°	Angle of fatigue critical point θ_2/°	Mean value of angle θ_m /°
D2	90	90	0	L_D1	116.6	121.8	115.9
				L_D2	110.8	114.2	
	90	90	45	L_D3	132.9	112.2	123.7
				L_D4	127.8	122.1	
	90	90	60	L_D7	117.7	135.3	123.8
				L_D8	118.5	123.6	
	90	90	90	L_D5	--	129.4	121.4
				L_D6	128.3	106.3	
	130	65	0	L_D9	106.1	118.6	110.6
				L_D10	112.3	105.2	
	130	65	45	L_D11	86.6	110.7	98.7
				L_D12	98.5	98.9	
	130	65	90	L_D13	--	89.5	94.8
				L_D14		100.1	
	55	110	0	L_D15	126.3	111.8	118.0
				L_D16	105.8	128.2	
	55	110	45	L_D17	118.1	110.5	117.4
				L_D18	105.4	135.6	
	55	110	90	L_D19	126.4	120.4	117.9
				L_D20	119.1	105.7	
Y	304	76	0	L_Y1	144.9	138.2	141.6
				L_Y2	--	--	
	197	91	0	L_Y4	138.7	154.7	143.7
				L_Y5	139.0	142.6	
	150	75	0	L_Y6	143.3	137.8	145.8
				L_Y7	152.9	149.2	
	150	75	45	L_Y8	133.6	156.5	144.5
				L_Y9	142.4	145.5	
	150	75	90	L_Y12	137.6	150.8	143.9

Type of notch	Maximum normal stress σ_{max}/MPa	Maximum shear stress τ_{max}/MPa	Phase angle φ/°	Specimen No.	Angle of fatigue critical point θ_1/°	Angle of fatigue critical point θ_2/°	Mean value of angle θ_m /°
				L_Y14	142.6	144.8	
	95	95	0	L_Y11	157.0	145.0	156.2
				L_Y13	172.9	149.7	
	95	95	45	L_Y15	147.3	150.2	147.7
				L_Y16	145.5	147.9	
	95	95	60	L_Y19	141.4	135.4	144.5
				L_Y20	146.5	151.8	
				L_Y21	146.0	146.1	
	95	95	90	L_Y17	146.7	153.2	152.5
				L_Y18	157.7	---	

Note: “---” means that no cracks were observed.

3 Introduction of the two methods

3.1 Stress field analysis near the notch

The principle stress directions of metallic notched specimens rotate during non-proportional fatigue loading, which results in the fact that the point with the maximum principal stress on the edge of notches changes constantly. Determining the location of the fatigue critical point is necessary because it is a key step in predicting the fatigue life for blunt notched specimens.

The thin-walled round tube notched specimens subjected to tension-torsion fatigue loading can be equivalent to two-dimensional notched specimens subjected to tensile-shear fatigue loading. For the circular hole notched specimens, the far-field stress is shown in Figure 7 where the notch radius of the circular hole is equal to a. The expression of the non-proportional loading is shown in the following Eq. (4):

$$\begin{aligned} \sigma &= \sigma_{\mathrm{a}} \sin(2\pi f t) + \sigma_{\mathrm{m}} \\ \tau &= \tau_{\mathrm{a}} \sin(2\pi f t + \varphi) + \tau_{\mathrm{m}} \end{aligned} \tag{4}$$

where σ_a and τ_a are the amplitude of normal stress and the amplitude of shear stress, respectively.

σ_m and τ_m are the mean value of normal stress and the mean value of shear stress, respectively. f is the frequency of fatigue loading, and φ is the phase angle.

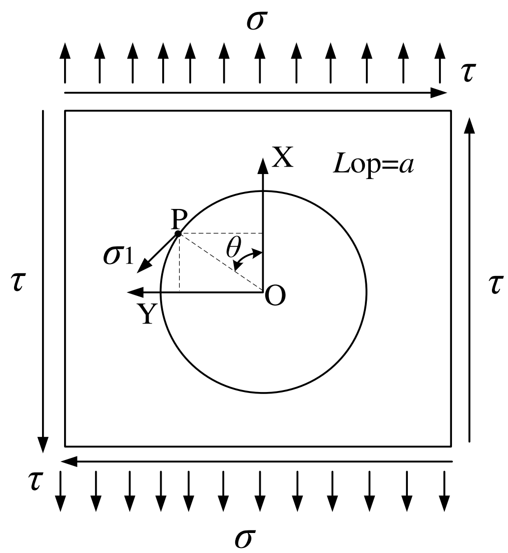

Fig.7 Schematic of two-dimensional circular notched specimens under multi-axial fatigue loading

In Figure 7, a polar coordinate system is established with the center of the circular hole being the origin. The direction of the normal stress is set as the polar diameter X-axis. The counterclockwise direction is set as the polar angle. P is a random point on the notch edge with coordinate (a,θ). The analytical solution of the stress field near the circular hole is shown in Eq. (5). The coordinate of point P is substituted into Eq. (5), and the stress components of point P are shown in Eq. (6). It can be seen from Eq. (6) that, even if the far-field stress is multi-axial, point P is still in the state of uniaxial stress.

$$\begin{Bmatrix} \sigma_{\mathrm{r}} \\ \sigma_\theta \\ \tau_{r\theta} \end{Bmatrix} = \begin{Bmatrix} \frac{\sigma}{2}\left(1-\frac{a^2}{r^2}\right)+\frac{\sigma}{2}\left(1-\frac{a^2}{r^2}\right)\left(1-3\frac{a^2}{r^2}\right)\cos 2\theta+\tau\left(1-\frac{a^2}{r^2}\right)\left(1-3\frac{a^2}{r^2}\right)\sin 2\theta \\ \frac{\sigma}{2}\left(1+\frac{a^2}{r^2}\right)-\frac{\sigma}{2}\left(1+3\frac{a^4}{r^4}\right)\cos 2\theta-\tau\left(1+3\frac{a^4}{r^4}\right)\sin 2\theta \\ -\frac{\sigma}{2}\left(1+2\frac{a^2}{r^2}-3\frac{a^4}{r^4}\right)\sin 2\theta-\tau\left(1-\frac{a^2}{r^2}\right)\left(1+3\frac{a^2}{r^2}\right)\cos 2\theta \end{Bmatrix} \tag{5}$$

$$\begin{Bmatrix} \sigma_{\mathrm{Pr}} \\ \sigma_{\mathrm{P}\theta} \\ \tau_{\mathrm{P}r\theta} \end{Bmatrix} = \begin{Bmatrix} 0 \\ \sigma-2\sigma\cos 2\theta-4\tau\sin 2\theta \\ 0 \end{Bmatrix} \Rightarrow \sigma_{1\mathrm{P}}=\sigma_{\mathrm{P}\theta}=\sigma-2\sigma\cos 2\theta-4\tau\sin 2\theta \tag{6}$$

Substitute Eq. (4) into Eq. (6) to obtain:

$$\begin{aligned}\sigma_{1p} &= \sigma - 2\sigma\cos 2\theta - 4\tau\sin 2\theta \\ &= A\sin(2\pi ft - \beta) + B\end{aligned} \tag{7}$$

where

$$\begin{aligned}A &= \sqrt{\left[(1-2\cos 2\theta)\sigma_a - 4\tau_a\sin 2\theta\cos\varphi\right]^2 + (4\tau_a\sin 2\theta\sin\varphi)^2} \\ \cos\beta &= \frac{(1-2\cos 2\theta)\sigma_a - 4\tau_a\sin 2\theta\cos\varphi}{A} \\ B &= \sigma_m - 2\sigma_m\cos 2\theta - 4\tau_m\sin 2\theta\end{aligned} \tag{8}$$

When $\sigma_m = \tau_m = 0$, Eq. (7) is reduced to the following equation:

$$\sigma_{1p} = A\sin(2\pi ft - \beta) \tag{9}$$

Generally, it is very difficult to calculate the analytical solution of the principal stress or the principal strain of the point on the notch edge. In the case of complex loadings or complex boundary conditions, the numerical solution of the first principal stress of the points on the notch edge can only be given by FEA. The constant amplitude non-proportional fatigue loading, as is shown in Eq. (4), is uniformly dispersed into *n* loading cases in a loading period, denoted as C_1-C_n. As is shown in Figure 8, each loading case C_i corresponds to an external loading (σ_i, τ_i). Finite element models of notched specimens can be achieved by placing *m* nodes on the notch edge and refining the grids at the notch root.

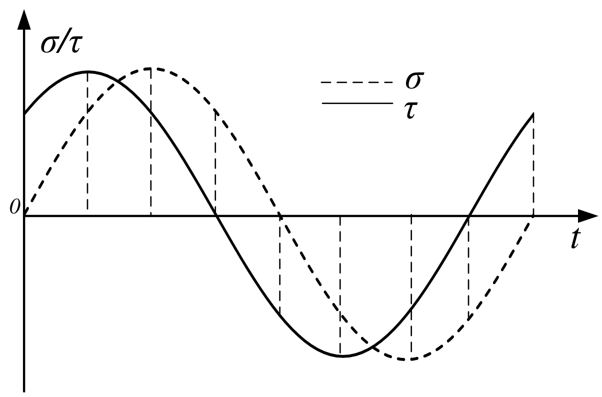

Fig.8 Schematic of uniformly dispersed multi-axial fatigue loading

3.2 Methods of predicting fatigue critical point

3.2.1 Method of stress amplitude

For metallic materials, stress-based parameters, strain-based parameters and energy-based parameters are commonly used to evaluate fatigue damage.[15] The stress-based damage parameters are generally used for high-cycle fatigue ($N>10^5$). Strain-based damage parameters are generally used for low-cycle fatigue ($N<10^5$). The energy-based damage parameters have certain physical significance from the perspective of energy accumulated in cyclic loading. Nevertheless, energy-based damage parameters are scalar and cannot explain the driving force of crack initiation.

Since the material is assumed to be within the range of linear elasticity in the paper, the strain-based damage parameters and stress-based damage parameters are equivalent. According to the Miner linear damage accumulation theory, the fatigue damage of one cyclic loading is defined as:

$$D = \frac{1}{N} \tag{10}$$

where N is the fatigue life.

The S-N curve expression of the material is:

$$S^{\alpha} N = C \tag{11}$$

where α and C are material constants and $\alpha > 0$.

Substitute Eq. (10) into Eq. (11) to obtain:

$$D = S^{\alpha} / C \tag{12}$$

According to Eq. (12) we can know that, for the same S-N curve, greater stress amplitude leads to severer fatigue damage.

According to Eq. (9), the mean value of local stress response spectrum of points on the notch edge line reaches zero when the mean value of far-field fatigue loading is zero, as is shown in Figure 9(a). In this case, according to the physical mechanism of fatigue damage in Eq. (12), greater stress amplitude leads to severer fatigue damage. Therefore, the point with the maximum stress amplitude on the notch edge is the fatigue critical point. As can be seen from Eq. (7), when the mean value of fatigue loading is non-zero, although each point on the notch edge is still in the uniaxial stress state, the mean stress of the local stress response spectrum at each point is different, as is shown in Figure 9(b). In this case, the local stress response spectrum of points on the notch edge needs to be modified, so that the mean stress of these points can be zero. The point with the maximum stress amplitude is taken as the fatigue critical point after the modification. At present, the Goodman's empirical formula is commonly used to modify the mean stress of engineering materials[1]:

$$\sigma_{a1}^{'} = \sigma_{a1}\left[1-\left(\frac{\sigma_{m1}}{\sigma_b}\right)\right] \tag{13}$$

where $\sigma_{a1}^{'}$ is the modified stress amplitude, σ_{a1} is the stress amplitude of the original local stress response spectrum, σ_{m1} is the mean stress of the original local stress response spectrum, and σ_b is the fracture strength.

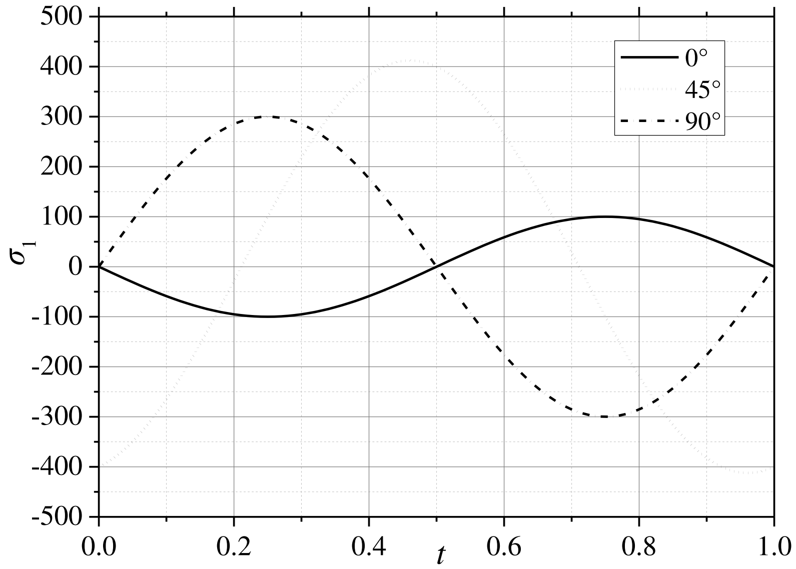

(a)σ_a=τ_a=100MPa， φ=90°， R=-1

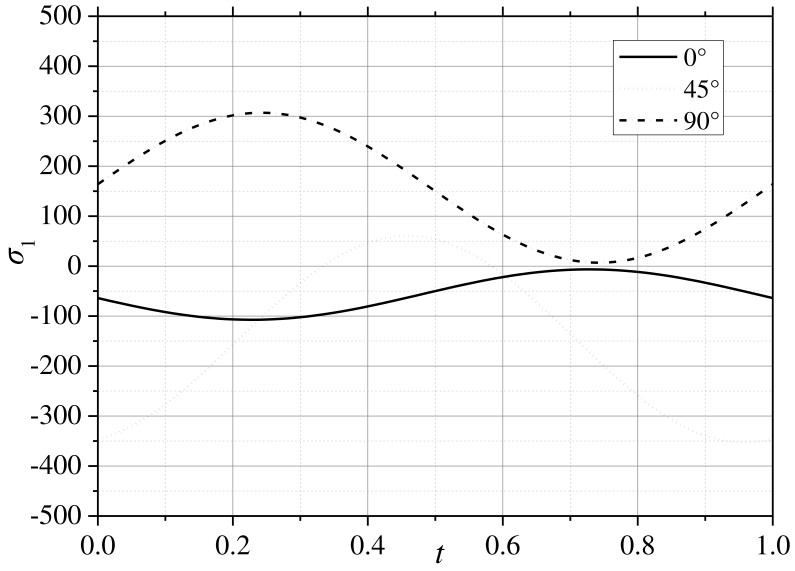

(b) $\sigma_a=\tau_a=100$MPa， $\varphi=90°$， $R=0$

Fig.9 the local stress response of three different points on the notch edge

3.2.2 Method of Susmel's parameter

The points on the notch edge are in uniaxial stress state, and the uniaxial stress state can be regarded as a special multi-axial stress state. Therefore, the multi-axial fatigue damage parameters can be used to characterize the fatigue damage of these points on the notch edge. Luo *et al.*[15] sorted out the commonly used multi-axial fatigue damage parameters in recent decades, and divided them into two categories: direct damage parameters and equivalent damage parameters. After that, 150 sets of multi-axial fatigue test data of 10 kinds of materials were collected to evaluate the accuracy of various multi-axial fatigue damage parameters. The results show that the Susmel's multi-axial fatigue damage parameter is suitable for most metallic materials. Susmel[16] took the plane bearing the maximum shear stress amplitude as the critical plane, which has certain physical significance. In addition, Susmel's multi-axial fatigue damage parameter can take the effect of mean stress on fatigue life into account.[17] Susmel's[16] multi-axial fatigue damage parameter is as follows:

$$\tau_{\mathrm{eq}} = \tau_{\mathrm{a}} + (t_{-1} - \frac{f_{-1}}{2})\frac{\sigma_{\mathrm{n}}^{\max}}{\tau_{\mathrm{a}}} \tag{14}$$

where τ_{a} is the shear stress amplitude on the critical plane, $\sigma_{\mathrm{n}}^{\max}$ is the maximum normal stress on the critical plane, f_{-1} and t_{-1} are the fully reversed axial fatigue limit and the fully reversed torsional fatigue limit, respectively. The local stress response of the points on the notch edge is in uniaxial stress state, so the angle of the plane bearing the maximum shear stress amplitude is 45°. According to Eq. (7), the stress amplitude and the mean stress at the point on the notch edge are A and B, respectively. Thus the following equations can be obtained:

$$\begin{aligned} \sigma_{\mathrm{n}}^{\max} &= \frac{(A+B)}{2} \\ \tau_{\mathrm{a}} &= \frac{A}{2} \end{aligned} \tag{15}$$

In this paper, the above two methods are used to predict the fatigue critical point of notched specimens. The first one is to directly compare the stress amplitude of these points on the notch edge (if the average stress is not zero, Goodman's empirical formula is used to do modification), which is called the stress amplitude method. The point with the maximum stress amplitude is the fatigue critical point. The other method is to calculate the Susmel's multi-axial fatigue damage parameter on the notch edge, which is called the Susmel's parameter method. The point with the maximum fatigue damage parameter is the fatigue critical point.

4 Predictive results of the two methods

4.1 The finite element models

Although the fatigue tests on notched specimens made of GH4169 nickel-base alloy are strain-controlled, the far-field stress is still within the elastic limit of material, and only the notch root enters plasticity. Therefore, the linear-elastic constitutive law is adopted in the finite element analysis of notched specimens made of GH4169 nickel-base alloy and 2297 aluminum-lithium alloy. For the circular hole notched specimens, the analytical solution of the stress field near notch can be obtained from Eq. (5). However, it is necessary to conduct finite element analysis on the waist-round hole notched specimens to obtain numerical solution of the stress field near notch.

The non-proportional fatigue loadings in Eq. (4) are dispersed into 16 loading cases uniformly, which is the same method adopted in Figure 8. Then, stress components in the vicinity of the notches are calculated under 16 kinds of loading cases by the software Patran 2012. The linear elastic constitutive law and 2D shell elements are used in FEA. The adopted minimum FE size is 0.025 mm in order to get precise stress field in the vicinity of notches. The finite element meshes near the notch are shown in Figure 10.

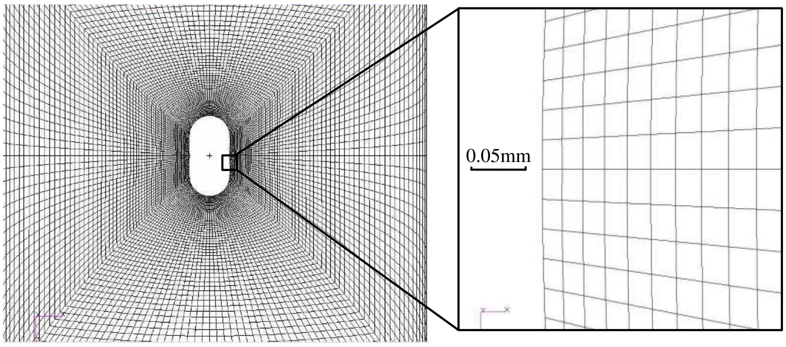

Fig.10 The finite element meshes near the notch

4.2 The comparison between experimental results and predictive results

The local stress response of the points on the notch edge of circular hole notched specimens can be calculated by Eq. (7). The local stress response of the points on the notch edge of the waist-round hole notched specimens is calculated by the linear-elastic finite element method. For the notched specimens made of GH4169 nickel-base alloy, the fatigue loading is a symmetric multi-axial loading, and the mean stress is zero. According to the amplitude stress method, the point with the maximum principal stress amplitude is the fatigue critical point. For the notched specimens made of 2297 aluminum-lithium alloy, the stress ratio R_2 of the multi-axial fatigue loading is equal to 0.1. It can be seen from Eq. (7) that the mean stress of the local stress response spectrum at different points on the notch edge line is different, so Eq. (13) can be used to modify the mean stress. The above two methods have been used to predict the fatigue critical point of notched specimens. The comparison between the test results and the predicted results of the fatigue critical point of the notched specimens made of GH4169 nickel-base alloy is shown in Table 5. The comparison between the test results and the predicted results of fatigue critical point of the notched specimens made of 2297 aluminum-lithium alloy is shown in Table 6. The mean values of absolute errors of the two methods are shown in Table 7.

According to Tables 5-7, we can find that both the two methods can accurately predict the fatigue critical point of metallic notched components under multi-axial fatigue loading. For the stress amplitude method, the maximum absolute error of notched specimens made of GH4169 nickel-base alloy is 9.2°, and the mean value of the absolute error is 4.07°. The maximum absolute error of notched specimens made of 2297 aluminum-lithium alloy is 13.5°, and the mean value of the absolute errors is 3.27°. For the Susmel's parameter method, the maximum absolute error of notched specimens made of GH4169 nickel-base alloy is 7.5° and the mean value of the absolute errors is 4.65°. The maximum absolute error of notched specimens made of 2297 aluminum-lithium alloy is 16.1° and the mean value of the absolute errors is 4.83°. In addition, the absolute error of the circular hole notched specimens is greater than that of the waist-round hole notched specimens for the above two methods. Because the analytical solution of the stress field in Eq. (5) is only an approximate solution of the stress field near the notch of thin-walled tube notched components, the original error is introduced.

It is very difficult to decide which of the two methods is better according to test data and predicted results. For the notched components under proportional fatigue loading, the predicted angles of two methods are same due to the fact that proportional loading is essentially uniaxial loading and the fatigue critical point is consistent with the failure point under static loading. In addition, since the points on the notch edge are in a state of uniaxial stress, the predictive accuracy is independent of phase angle of multi-axial fatigue loading. The predictive errors are determined by the dispersion of materials and smaller dispersion leads to a higher prediction accuracy.

Table5 Comparison between test results and predicted results of fatigue critical point of notched specimens made of GH4169 nickel-base alloy

Type of notch	Specimen No.	Phase angle φ/°	Experimental value /°	Predicted value /°		Absolute error /°	
				Method of σ_{a1}	Method of τ_{eq}	Method of σ_{a1}	Method of τ_{eq}
D1	GD1_1&GD1_2	0	93.6	90.0	90.0	3.6	3.6
	GD1_3&GD1_4	0	128.0	135	135.0	7.0	7.0
	GD1_5&GD1_6	45	98.0	101.5	106.2	3.5	8.2
	GD1_7&GD1_8	45	111.4	114.7	115.1	3.3	3.7
	GD1_9&GD1_10	90	95.0	90.4	96.4	4.6	1.4
D2	GD2_1&GD2_2	0	97.5	90.0	90.0	7.5	7.5
	GD2_3&GD2_4	0	44.0	45.0	45.0	1.0	1.0
	GD2_5&GD2_6	45	104.2	101.5	106.2	2.7	2.0
	GD2_7&GD2_8	45	110.3	114.7	115.1	4.4	4.8
	GD2_9&GD2_10	90	99.6	90.4	96.4	9.2	3.2
Y	GY_1&GY_2	0	40.2	40.0	41.2	0.2	1.0
	GY_3&GY_4	0	148.5	155.0	146.5	6.5	2.0
	GY_5&GY_6	45	144.7	142.3	145.2	2.4	0.5
	GY_7&GY_8	45	145.5	144.6	143.1	0.9	2.4
	GY_9&GY_10	90	143.3	139.0	142.6	4.3	0.7

Table6 Comparison between test results and predicted results of fatigue critical point of notched specimens made of 2297 aluminum-lithium alloy

Type of notch	Specimen No.	Phase angle φ/°	Experimental value /°	Predicted value /°		Absolute error /°	
				Method of σ_{a1}	Method of τ_{eq}	Method of σ_{a1}	Method of τ_{eq}
D2	L_D1&L_D2	0	115.9	121.7	122	5.8	6.1
	L_D3&L_D4	45	123.7	122.0	121	1.7	2.7
	L_D7&L_D8	60	123.8	122.7	126	1.1	2.2
	L_D5&L_D6	90	121.4	124.7	124	3.3	2.6
	L_D9&L_D10	0	110.6	112.3	112	1.7	1.4
	L_D11&L_D12	45	98.7	111.7	112	13	13.3
	L_D13&L_D14	90	94.8	108.3	102	13.5	7.2

Type of notch	Specimen No.	Phase angle φ/°	Experimental value /°	Predicted value /°		Absolute error /°	
				Method of σ_{a1}	Method of τ_{eq}	Method of σ_{a1}	Method of τ_{eq}
	L_D15&L_D16	0	118.0	128.0	128	10	10
	L_D17&L_D18	45	127.4	128.7	130	1.3	2.6
	L_D19&L_D20	90	117.9	130.3	134	12.4	16.1
Y	L_Y1&L_Y2	0	141.6	144.8	144.5	3.2	2.9
	L_Y4&L_Y5	0	143.7	146.4	146.5	2.7	2.8
	L_Y6&L_Y7	0	145.8	146.4	146.5	0.6	0.7
	L_Y8&L_Y9	45	144.5	146.3	146.5	1.8	2
	L_Y12&L_Y14	90	143.9	146.5	146.5	2.6	2.6
	L_Y11&L_Y13	0	156.2	150.0	149.8	6.2	6.4
	L_Y15&L_Y16	45	147.7	148.0	151.4	0.3	3.7
	L_Y19&L_Y20 &L_Y21	60	144.5	150.2	149.8	5.7	5.3
	L_Y17&L_Y18	90	152.5	151.0	151.4	1.5	1.1

Table7 The mean value of absolute errors for two kinds of metallic notched specimens

Methods	GH4169 nickel-base alloy				2297 aluminum-lithium alloy		
	D1 /°	D2 /°	Y /°	All specimens /°	D2 /°	Y /°	All specimens /°
Method of σ_{a1}	4.40	4.96	2.86	4.07	6.38	2.73	4.65
Method of τ_{eq}	4.78	3.70	1.32	3.27	6.42	3.06	4.83

5 Conclusion

Two methods based on local stress response, (the stress amplitude method and the Susmel's parameter method), are proposed to locate the fatigue critical point of notched components under multi-axial fatigue loading. Multi-axial fatigue tests were carried out on the notched specimens made of GH4169 nickel-base alloy and 2297 aluminum-lithium alloy. After the fatigue tests, the angle of the fatigue critical point of the notched specimens was measured through optical microscope. The predicted results show that both methods can accurately predict the angle of fatigue critical point. The main conclusions are as follows:

(1) Both the radius of fatigue damage field in the SFI and the critical distance in the TCD are

vectors. The origin of the vector is the fatigue critical point. Therefore, determining the fatigue critical point of notched parts is the basis of applying these two methods to predict the fatigue life of notched specimens under multi-axial fatigue loading.

(2) For notched components under non-proportional fatigue loading, although the far-field stress is multi-axial, points on the notch edge are still in the uniaxial stress state. The direction of the first principal stress is the tangential direction of each point.

(3) For the stress amplitude method, when the mean value of the fatigue loading is zero, the mean value of the local stress response spectrum of points on the notch edge is also zero. The point with the maximum stress amplitude is the fatigue critical point. When the mean value of fatigue loading is non-zero, the mean value of the local stress response spectrum of points on the notch edge is also non-zero. Moreover, the mean stress at different points on the notch edge is different. Therefore it is necessary to modify the mean stress to locate the point with the maximum fatigue damage.

(4) For the Susmel's parameter method, the uniaxial stress state of the point on notch edge is regarded as a special multi-axial stress state to calculate the fatigue damage. Susmel's multi-axial fatigue damage parameter takes the effect of mean stress on fatigue damage into consideration.

6 Acknowledgement

National Science and Technology Major Project (2017-Ⅵ-0003-0073) are acknowledged for supporting the present research work.

7 References

[1] Yao WX. Fatigue life estimation of structures. Beijing: National defense industry press, 2019.

[2] Singh MNK, Glinka G, Dubey RN. Elastic-plastic stress-strain calculation in notched bodies subjected to non-proportional loading. *Int J Fract*. 1996, 76(1):39-60.

[3] Yao WX. Stress field intensity approach for predicting fatigue life. *Int J Fatigue*. 1993; 15(3):243-246.

[4] Shang DG. Local stress–strain field intensity approach to fatigue life prediction under random cyclic loading. *Int J Fatigue*. 2001; 23(10):903-910.

[5] Li Y, Yao WX, Wen WD. Application of stress field intensity for the prediction of multiaxial fatigue. *J Mechanical Strength*. 2002; 24(2): 258–261.

[6] Tanaka K. Engineering formulae for fatigue strength reduction due to crack-like notches. *Int J of Fract*. 1983; 22(2):39-46.

[7] Taylor D. Geometrical effects in fatigue: a unifying theoretical mode. *Int J Fatigue*. 1999; 21(5):413-420.

[8] El Haddad MH, Dowling NE, Topper TH, Smith KN. J integral applications for short fatigue cracks at notches. *Int J Fract*. 1980; 16(1):15-30.

[9] Chaves V, Beretta G, Balbín JA, Navarro A. Fatigue life and crack growth direction in 7075-T6 aluminium alloy. *Int J Fatigue*. 2019; 125(8): 222-236.

[10] Susmel L. Multiaxial notch fatigue: From nominal to local stress/strain quantities. London:CRC Press, 2009.

[11] Gates N, Fatemi A. Notch deformation and stress gradient effects in multiaxial fatigue. *Theor and Applied Fract Mechanics*. 2016; 84(8): 3-25

[12] Wang YY. Multiaxial fatigue behavior and life estimation of metallic materials. Nanjing: Nanjing university of aeronautics and astronautics, 2005.

[13] Xia TX. Field strength method for predicting multiaxial fatigue life of structures. Nanjing: Nanjing university of aeronautics and astronautics, 2016.

[14] Luo P, Yao WX, Li P. A notch critical plane approach of multiaxial fatigue life prediction for metallic notched specimens. *Fatigue Fract Eng Mater Struct*. 2019; 42(4):854-870.

[15] Luo P, Yao WX, Susmel L, Wang YY, Ma XX. A survey on multiaxial fatigue damage parameters under non-proportional loadings. *Fatigue Fract Eng Mater Struct*. 2017; 40(9):1323-1342.

[16] Susmel L, Lazzarin P. A bi-parametric Wöhler curve for high cycle multiaxial fatigue assessment. *Fatigue Fract Eng Mater Struct*. 2010; 25(1):63-78.

[17] Susmel L, Tovo R, Lazzarin P. The mean stress effect on the high-cycle fatigue strength from a multiaxial fatigue point of view. *Int J Fatigue*. 2005; 27(8):928-943.